Polarization singularities of biological tissues images

O. V. Angelsky
A. G. Ushenko
Y. G. Ushenko
Y. Y. Tomka
Chernivtsi National University
2 Kotsyubinsky Str.
Chernivtsi, 58012, Ukraine

Abstract. The ways to the polarization singularities of the biological tissues images of various morphological structures have been theoretically analyzed. The coordinate distributions of singly (linear states of polarization) and doubly degenerated (circular states of polarization) polarization singularities of the physiologically normal and pathologically changed biological tissues have been experimentally examined. The statistical criteria of diagnostics of the kidney tissue collagenous disease (the third and the fourth statistical moments of the linear density singularity points) have been determined. It was discovered that the process of the pathological change of the kidney tissue morphology leads to the formation of the self-similar (fractal) coordinate distribution of the polarization singularities of its image. [DOI: 10.1117/1.2360527]

Keywords: polarization singularity; biological tissue; statistics; statistical moments; power spectrum.

Paper 06013R received Jan. 27, 2006; revised manuscript received May 23, 2006; accepted for publication Jun. 21, 2006; published online Oct. 17, 2006.

1 Introduction

Traditionally the description of the polarization state of optical fields is based on the definition of the coherency matrix of light oscillations, which is univocally connected with the Stokes vector parameters in every point of such a field.[1,2] According to such an approach, the main state of polarization turns out to be an elliptically polarized wave with main half axes a, b. Boundary (singular[3]) states of such polarization are linear $[(a=0, b\neq 0), (a\neq 0, b=0)]$ and circular $(a=b)$ light oscillations. It is shown in Refs. 4–12 that such points of singularities of the optical field form its structure, determining in such a way its polarization properties.

On the other hand, practically all the investigations of polarization singularities of optical fields are of theoretical nature and are being led separately from certain optical-geometric properties of objects forming such fields. One of the examples of polarizationally active physical structures is a biological tissue, formed by a birefringent, geometrically self-similar architectonic matrix.[13] Thus the search for the conditions of the formation of polarization singularities by such objects and experimental investigation of the peculiarities (statistic, stochastic, or fractal ones)[14] of the structure of the coordinate distributions of the polarization singularities of the biological tissues images for the purpose of a possible usage of such information in the diagnostics of their physiological state is topical.

2 Biological Tissues as the "Generators" of Polarization Singularities

In Refs. 15–20 the efficiency of matrix model for the description of polarization properties of biological tissues is theoretically substantiated and experimentally proved. Within such an approach, the biological tissue is regarded as a two-component amorphous-crystalline structure. The amorphous component is optically isotropic while the crystalline one is formed by optically uniaxial protein fibrils (Fig. 1), that is, it is anisotropic.

The process of forming a polarization structure of a biological tissue image is described by the matrix relation

$$S(\alpha,\beta) = \{\mathbf{F}\} S_o(\alpha_0,\beta_0), \tag{1}$$

in which $S_o(\alpha_0,\beta_0)$, $S(\alpha,\beta)$ are the Stokes vectors of the illuminating and object field; $\{\mathbf{F}\}$ is Mueller matrix for optically uniaxial birefringent fibrils; α_0, β_0 are azimuth and ellipticity of the light oscillations polarizing the illuminating beam.

Equation (1) is written in full as follows:

$$\begin{pmatrix} 1 \\ \cos 2\alpha \cos 2\beta \\ \sin 2\alpha \cos 2\beta \\ \sin 2\beta \end{pmatrix} = \begin{Vmatrix} 1 & 0 & 0 & 0 \\ 0 & f_{22} & f_{23} & f_{24} \\ 0 & f_{32} & f_{33} & f_{34} \\ 0 & f_{42} & f_{43} & f_{44} \end{Vmatrix} \times \begin{pmatrix} 1 \\ \cos 2\alpha_0 \cos 2\beta_0 \\ \sin 2\alpha_0 \cos 2\beta_0 \\ \sin 2\beta_0 \end{pmatrix}. \tag{2}$$

Here α, β are azimuth and ellipticity of light oscillations polarization, determined by the principal half axes of the polarization ellipsis

$$\alpha = \Theta(a=0) - 0.5\pi, \tag{3}$$

Address all correspondence to A. G. Ushenko, Chernivtsi National University, 2 Kotsyubinsky Str., Chernivtsi, 58012, Ukraine; E-mail: ushenko-bio@itf.cv.ua

1083-3668/2006/11(5)/054030/9/$22.00 © 2006 SPIE

$$\beta = \pm \arctan\left(\frac{b}{a}\right), \tag{4}$$

where Θ is the rotation angle of the passing axis of the analyzer of the orthogonal orientation of the larger half axis a.

All the elements of Mueller matrix are given in such expressions

$$f_{22} = \cos^2 2\rho + \sin^2 2\rho \cos\delta,$$

$$f_{23} = f_{32} = \cos 2\rho \sin 2\rho(1 - \cos\delta),$$

$$f_{24} = -f_{42} = -\sin 2\rho \sin\delta, \quad f_{33} = \sin^2 2\rho + \cos^2 2\rho \cos\delta,$$

$$f_{34} = -f_{43} = \cos 2\rho \sin\delta, \quad f_{44} = \cos\delta. \tag{5}$$

Here ρ is the orientation of optical axis of the birefringent fibril; δ is the value of phase shift between the components of the light-wave amplitude.

Such a simulation of the polarization properties of a biological tissue under the conditions of single scattering enables us to determine the univocal interrelation between the optical-geometric structure $[\rho(x,y), \delta(x,y)]$ of its architectonics and by the state of polarization (α, β) of light oscillations in every point (x,y) of its image

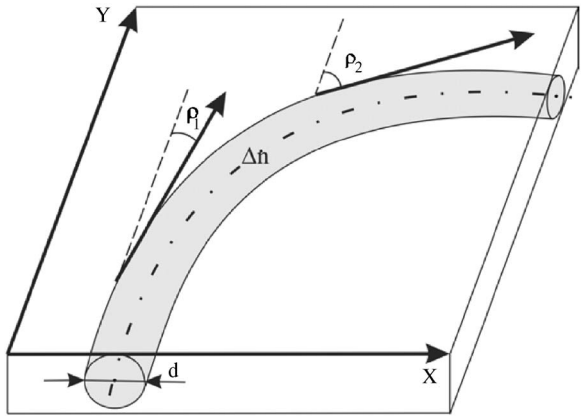

Fig. 1 The birefringent (Δn) curvilinear optically uniaxial fibril (ρ_i—angles of fibril arranging, d—geometrical cross-section of the fibril).

$$\alpha = 0.5 \arctan\left(\frac{f_{32}\cos 2\alpha_0 \cos 2\beta_0 + f_{33}\sin 2\alpha_0 \cos 2\beta_0 + f_{34}\sin 2\beta_0}{f_{22}\cos 2\alpha_0 \cos 2\beta_0 + f_{23}\sin 2\alpha_0 \cos 2\beta_0 + f_{24}\sin 2\beta_0}\right), \tag{6}$$

$$\beta = 0.5 \arcsin(f_{42}\cos 2\alpha_0 \cos 2\beta_0 + f_{43}\sin 2\alpha_0 \cos 2\beta_0 + f_{44}\sin 2\beta_0). \tag{7}$$

For the geometry of architectonics of a real biological tissue, the wide range of orientation ($0 \le \rho \le \pi$) and phase ($0 \le \delta \le 2\pi$) changing parameters are characteristic.[21] Therefore, [see Eqs. (5) to (7)] the "generation" of singular points by such an object appears to be quite probable

$$\begin{cases} \beta = 0 \leftrightarrow \delta = 2q\pi, \quad q = 0,1,2,\ldots, \\ 0 \le \alpha \le \pi, \end{cases} \tag{8}$$

$$\begin{cases} \beta = \pm 0.25\pi \leftrightarrow \delta = \pm 0, \quad 5\pi + 2q\pi, \\ \alpha = 0, \end{cases} \tag{9}$$

which determine the coordinate structure and boundaries of changes in the state of its image polarization.

Solving Eqs. (5) and (7) and taking into account Eqs. (8) and (9) gives the following conditions of forming polarization singularities by birefringent (ρ, δ) fibrils of biological tissue being illuminated by an elliptically polarized (α_0, β_0) wave

$$\sin 2(\rho - \alpha_0) = \tan 2\beta_0 \operatorname{cotan}\delta, \tag{10}$$

$$\sin 2(\rho - \alpha_0) = \frac{\pm 1 - \cos\delta \sin 2\beta_0}{\cos 2\beta_0 \sin\delta}. \tag{11}$$

Particular conditions of forming the linear ($\delta = 2q\pi \rightarrow \beta = 0, q = 0,1,2,\ldots$) and circular ($\delta = 0.5\pi + 2q\pi \rightarrow \beta = 0.25\pi$) singularities of polarization by biological tissue being illuminated either by plane

$$\beta_0 = 0, \quad 0 \le \alpha_0 \le \pi \rightarrow \begin{cases} \rho = \alpha_0, \\ 0 \le \delta \le 2\pi, \end{cases} \tag{12}$$

$$\beta_0 = 0, \quad 0 \le \alpha_0 \le \pi \rightarrow \begin{cases} \rho = \alpha_0 \pm 0.25\pi, \\ \delta = \pm 0,\ 5\pi. \end{cases} \tag{13}$$

or by a circularly polarized wave

$$\beta_0 = \pm 0.25\pi, \quad 0 \le \alpha_0 \le \pi \rightarrow \begin{cases} 0 \le \rho \le \pi, \\ \delta = \pm 0,\ 5\pi, \end{cases} \tag{14}$$

$$\beta_0 = \pm 0.25\pi, \quad 0 \le \alpha_0 \le \pi \rightarrow \begin{cases} 0 \le \rho \le \pi, \\ \delta = 2q\pi,\ q = 0,\ 1,\ 2,\ \ldots \end{cases} \tag{15}$$

can be revealed from Eqs. (10) and (11).

"Generation" of polarization singularities is quantitatively illustrated by the results of the computer simulation of the

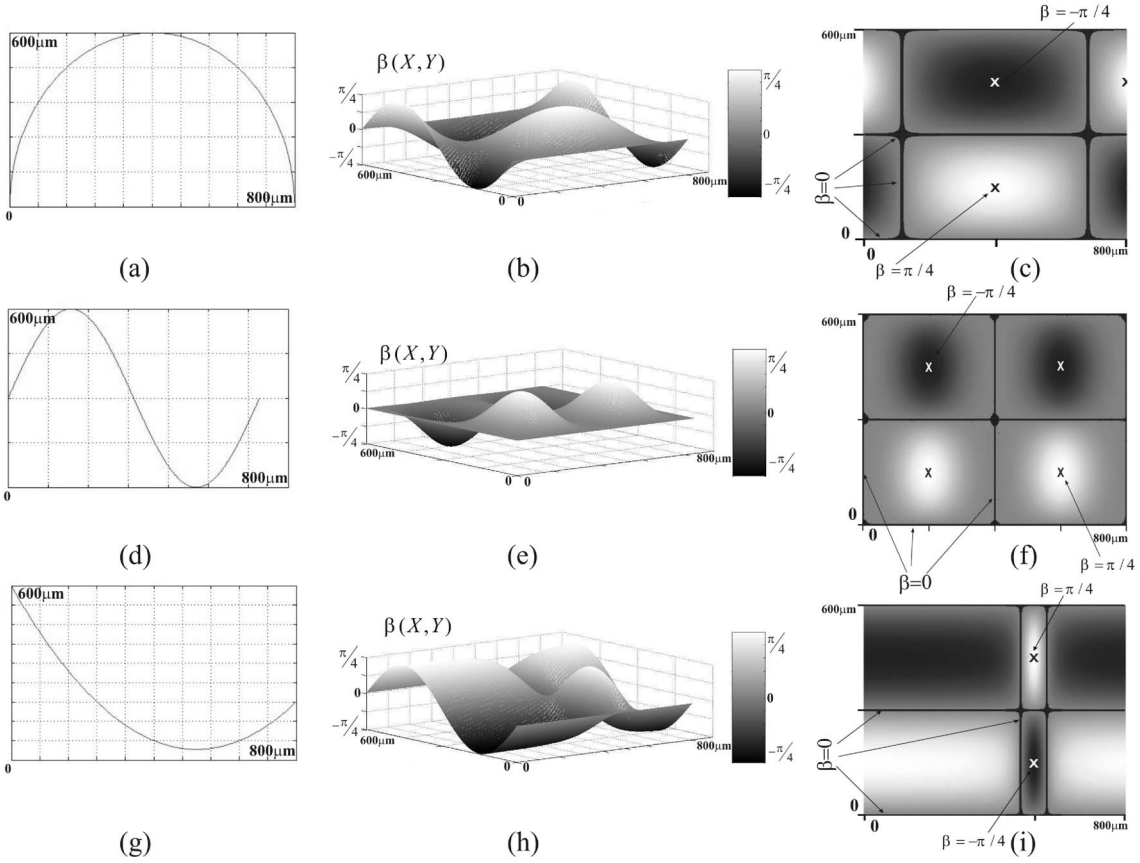

Fig. 2 The coordinate distributions of the ellipticity of light oscillation polarization (b), (e), (h) of different types of curvilinear birefringent fibrils arrangement (a), (d), (g) and the network of their polarization singularities (c), (f), (i).

polarization image of the curvilinear birefringent ($\Delta n=1$, 5×10^{-3}) fibrils set (Fig. 2). The left column of Fig. 2 depicts the different types [semicircle (a), sine curve (d), and complex parabola (g)] of fibrils arrangement. The central column [(b), (e), (h)] illustrates the coordinate distributions of the ellipticity $\beta(X,Y)$ of light oscillations polarization, the values of ellipticities are shown in grayscales. The coordinate distributions of polarization singularities [$\beta(X,Y)=0$ and $\beta(X,Y)=\pm0.25\pi$] are depicted in the right column [(c), (f), (i)].

It can be seen from the data obtained that the change in the geometry of the fibrils packing in the plane of the biological tissue layer [fragments (a), (d), (g)] shows in the change of coordinate distribution of the points of polarization singularities [fragments (c), (f), (i)] of its polarization ellipses [fragments (b), (e), (h)]. Thus to analyze the images of real biological structures, one can use not all the information about their polarization structure,[22] but only the information concerning coordinate distributions of singly and doubly degenerative points.

3 The Technique of the Polarization Singularities Detection

The optical arrangement of measuring the biological tissue polarization structure is given in Fig. 3. The illuminating has been arranged by the collimated beam ($\varnothing=10^4$ μm) of a He-Ne laser ($\lambda=0.6328$ μm, $W=5.0$ mW). The polarization illuminator consisted of quarter wave plates 3 and 5 and polarizer 4 forms the illuminating beam with an arbitrary azimuth of $0\le\alpha_0\le\pi$ or with the polarization ellipticity of $0\le\beta_0\le0.5\pi$.

The polarization images of the biological tissue were projected into the plane of a light-sensitive area (800×600) of charge-coupled device (CCD) camera 10 with the help of microscope objective 7. This provides the measuring range of structural elements of the biological tissue for the following scales 2 to 2000 μm.

The conditions of experiment were chosen in such a way that it enabled us to reduce the space-angular aperture filtering while forming the biological tissues images. This was ensured by the conformance of angular characteristics of indicatrixes of light scattering by the biological tissues samples ($\mathbf{\Omega}\approx16^0$) and the angular aperture of the microobjective ($\Delta\omega=20^0$). Here $\mathbf{\Omega}$ is the solid angle within which 98% of all energy of light-scattered radiation is concentrated.

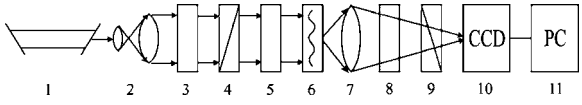

Fig. 3 Experimental setup. 1—He-Ne laser; 2—collimator; 3, 5, 8—quarter wave plates; 4, 9—polarizer and analyzer, respectively; 6—object of investigation; 7—microobjective; 10—CCD camera; 11—personal computer.

The analysis of the biological tissue images was performed by the quarter wave plate 8 and polarizer 9.

The methods of determining the coordinate distribution of the polarization singularities of the biological tissue image consist of the following sequence of actions:

1. The minimum and maximum levels of the image intensity for each separate pixel (m,n) of the CCD camera, $I_{min}(r_{m,n})$, $I_{max}(r_{m,n})$, and the corresponding rotation angles, $\Theta(r_{m,n})[I(r_{m,n}) \equiv I_{\min}]$, are determined by rotating an axis of the analyzer transmission 8 in the limits of $\Theta = 0 - \pi$.
2. The polarization map (in other words, two-dimensional distributions of azimuth and ellipticity values of polarization) of the biological tissue image has been calculated in accordance with the following relations:

$$\alpha(r_{m,n}) = \Theta[I(r_{m,n}) \equiv I_{\min}] - \frac{\pi}{2},$$

$$\beta(r_{m,n}) = \arctan \frac{I(r_{m,n})_{\min}}{I(r_{m,n})_{\max}}. \tag{16}$$

3. The polarization map of points with linear polarization [of the Eqs. (10) and (12)] has been determined as

$$\delta(r_{m,n}) = \arctan\left[\frac{\tan 2\beta(r_{m,n})}{\tan \alpha(r_{m,n})}\right] = 2q\pi,$$

$$\beta(r_{m,n}) = 0. \tag{17}$$

4. The polarization map of points with circular polarization [of the Eqs. (11) and (13)] has been determined as

$$\delta(r_{m,n}) = \arctan\left[\frac{\tan 2\beta(r_{m,n})}{\tan \alpha(r_{m,n})}\right] = 0.5\pi + 2q\pi,$$

$$\beta(r_{m,n}) = 0.25\pi. \tag{18}$$

4 Objects of Investigation Characteristics

The histological sections of the biological tissue of various morphological structures were used as the investigating objects:

- Muscular tissue (myocardium)— MT [Figs. 4(a) and 4(b)]
- Large intestine wall tissue—IT [Figs. 4(c) and 4(d)].

The presence of an anisotropic component[15] with a birefringence index of its substance $\Delta n \approx 1.5 \times 10^{-2}$ is similar to the chosen investigated objects. Visualized images of such structures in the crossed polarizer and analyzer are given in Figs. 4(b) and 4(d).

The geometric thickness of the biological tissue of both types was 50 to 60 μm.

Such optical geometric parameters of the biological tissue sample provided the conditions of a single scattering (an index of the attenuation of τ radiation by the layer of d—thickness was not over 0.01). Herewith the phase-shift value of such layers did not exceed one full period of $0 \leq (2\pi/\lambda)\Delta n d \leq 2\pi$.

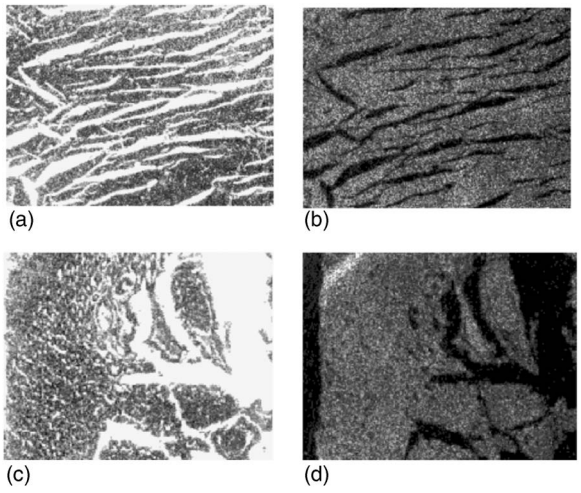

Fig. 4 Polarization images of the muscular (myocardium) (a), (b) and the large intestine wall (c), (d) tissue histological sections. The fragments (a), (c) correspond to the situation of the coaxial polarizer and analyzer; (b) and (d) correspond to the situation of crossed polarizer and analyzer.

The morphological structure of the architectonics of such biological tissues is various. The MT is formed by the "quasiordering" beams of the birefringent myosin bundles [Fig. 4(b)]. The IT tissue includes "island" insertions of an anisotropic collagen [Fig. 4(d)].

5 Analysis and Discussion of the Experimental Data

This section contains the following data:

- Phase maps (two-dimensional distributions of phase-shift values) $\delta(r_{m,n})$ of physiologically normal biological tissue images (Figs. 5, 6, and 9) and pathologically changed ones (Fig. 10).
- Coordinate distributions of singly degenerated $\delta(r_{m,n}) = 0$ and doubly degenerated $\delta(r_{m,n}) = 0.5\pi$ polarization singularities of all types of the biological tissue images (Figs. 7 and 11).
- Probability densities $N(m)$ of the singularity points of the polarization images of the kidney tissues (Fig. 12).

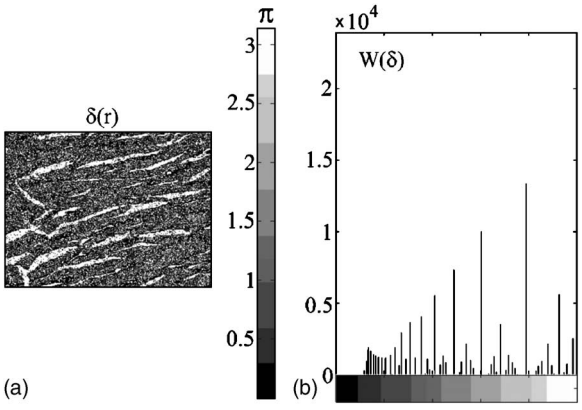

Fig. 5 The coordinate (a) and probability (b) distributions of the phase shifts δ of the muscular tissue polarization image.

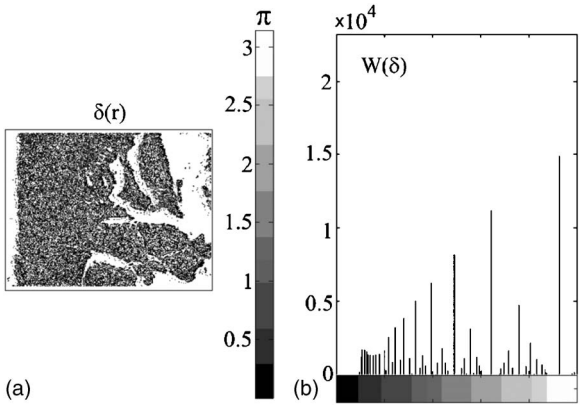

Fig. 6 The coordinate (a) and probability (b) distributions of the phase shifts δ of the large intestine wall polarization image.

- Autocorrelation functions $G_{xx}(\delta)$ of the phase maps of the physiologically normal and pathologically changed kidney tissue (Fig. 13).
- Log-log dependencies of power spectrum of the polarization singularities density of the physiologically normal and pathologically changed kidney tissue images (Figs. 14 and 15).

5.1 *Coordinate and Statistical Structure of the Phase Maps of the Biological Tissue Polarization Images*

The coordinate distributions of the phase values $\delta(r)$ of the biological tissue polarization images of both types are given in Fig. 5 (myocardium tissue) and Fig. 6 (large intestine wall tissue).

It can be seen from the obtained data that the range of the phase shift changing $\delta(r)$ for all images is wide enough and is in the range of 0.05π to 2π [Fig. 5(a) and Fig. 6(a)]. Such a big interval of changing values of $\delta(r)$ could be connected with different thicknesses of optically anisotropic protein

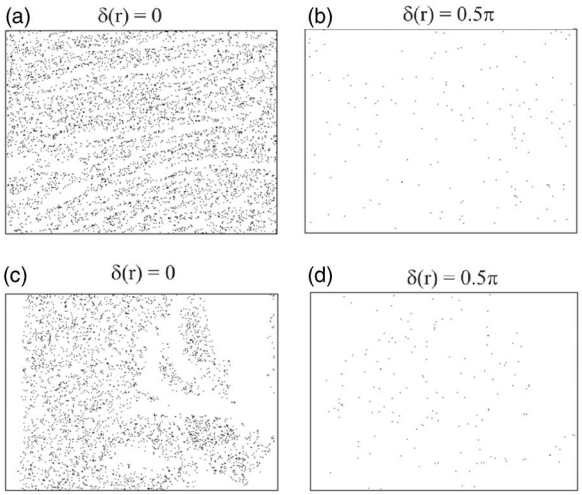

Fig. 7 The coordinate distributions of singly (a), (c) and doubly (b), (d) degenerated polarization singularities of the muscular tissue image (a), (b) and of the large intestine wall image (c), (d).

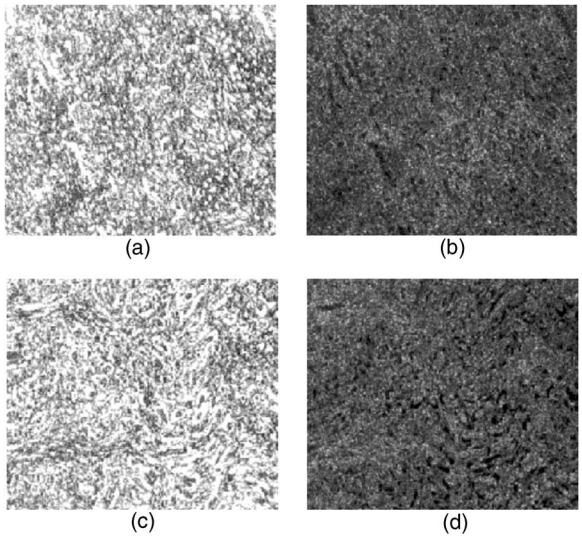

Fig. 8 The polarization images of the histological sections of the physiologically normal (a), (b) and pathologically changed (c), (d) kidney tissue. The fragments (a), (c) correspond to the situation of the coaxial polarizer and analyzer; (b), and (d) correspond to the situation of crossed polarizer and analyzer.

structures of the biological tissue (myosin and collagen). It is also seen from two-dimensional structure of $\delta(r)$ parameter that the phase maps of both images "are formed" by the ensemble of local phase domains $[\delta_i(r) \approx \text{const}]$ of different shape and size. The statistically discrete character of a phase-shifting ability of MT and IT sample substances characterize the ensemble of local extrema of histograms $W(\delta)$ [Fig. 5(b) and Fig. 6(b)].

The main differences in the phase maps of the examined biological tissue patterns consist in the coordinate heterogeneity of the parameter distribution $\delta(r)$ [Fig. 5(a) and Fig. 6(a)] and also in a greater density of the extrema of the phase-shift probability values in the field of 0.05π to 0.3π for the IT tissue images [Fig. 6(b)] in comparison with the similar statistics of $\delta(r)$ changing for MT images [Fig. 5(b)]. Such results could be connected with a different optical-geometric morphological structure of the mentioned tissues. The island insertions of optically anisotropic collagen of IT biological tissue form separate large-scaled phase domains of (200 to 300 μm). The MT phase map is formed by sufficiently ordered areas $\delta_i(r) \approx \text{const}$ and the corresponding directions of the myosin fibers placing. A statistically larger MT phase-shifting ability [Fig. 5(b)] might be connected with a higher concentration of the myosin fibrils in MT layer plane in comparison with the local collagen formations in IT tissue [Fig. 6(b)].

The obtained data concerning the phase structure of the polarization heterogeneous images of the biological tissue were put into the fundamentals of studying according to conditions (10), (12), (11), and (13) coordinate distributions of singly $\delta(r_{m,n})=0$ [Figs. 7(a) and 7(c)] and doubly $\delta(r_{m,n})=0.5\pi$ [Figs. 7(b) and 7(d)] degenerated singularity points of polarization.

The analysis of the information obtained showed that the biological tissue images of a different morphological structure

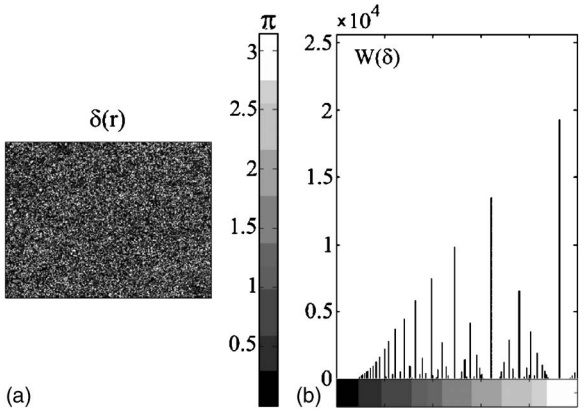

Fig. 9 The coordinate (a) and probability (b) distributions of the phase shifts δ of the physically normal kidney tissue polarization image.

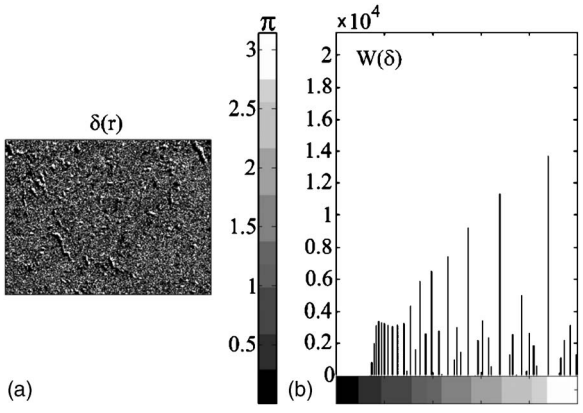

Fig. 10 The coordinate (a) and probability (b) distributions of the phase shifts δ of the kidney tissue polarization image with early symptoms of the collagenous disease.

have sufficiently "developed" nets of the polarization singularities. The probability of forming doubly degenerated polarization singularities [Figs. 7(b) and 7(d)] is far less than for singly degenerated ones [Figs. 7(a) and 7(c)]. Such a peculiarity could be connected with the fact that the realization of the conditions (10) and (12) is more probable in comparison with the conditions (11) and (13). Besides, the optically isotropic sections of the biological tissue do not change the polarization condition of the illuminating laser beam (in our case, $\alpha_0 = 0.25\pi$, $\beta_0 = 0$).

The coordinate structure of the polarization singularities of MT image [Figs. 7(a) and 7(b)] corresponds in general to the directions of the optically anisotropic myosin bundles placements [Figs. 4(a) and 4(b)]. For the IT tissue image [Figs. 4(c) and 4(d)], more equiprobable distribution of the polarization singularities [Figs. 7(c) and 7(d)] has been determined. The densities of singularly polarized points of the examined biological tissue sample images also differ.

The discovered coordinate and quantitative differences of the net structure in the polarization singularities of the biological tissue images were put into the fundamentals of early (preclinical) diagnostics of the physiological condition of the kidney tissue.

5.2 *Polarization-Singular Diagnostics of the Biological Tissue*

Optically thin ($\tau \leq 0.1$) histological sections of a healthy [Figs. 8(a) and 8(b)] and pathologically changed kidney (an early stage of collagenous disease—the enlargement of the connective tissue) [Figs. 8(c) and 8(d)] have been used as the objects of the investigation. From the medical point of view, the selected kidney tissue samples are practically identical—the traditional histochemical methods do not reveal any differences between of them. The comparative analysis of the images [Figs. 8(a) and 8(c)] obtained in the coaxial polarizer 4 and analyzer 8 (Fig. 3) confirms the identity of their morphological structure. The polarization contrasted (crossed polarizer-analyzer) images of the connective tissue collagen net [Figs. 8(b) and 8(d)] are characterized by a slightly higher "clearance" level for the pathologically changed sample. This fact proves visually that there is a greater extent of anisotropy of the kidney tissue substance with early symptoms of collagenous disease. The phase maps of sample images (Figs. 9 and 10) quantitatively show polarization properties of the samples of both types. One can see that the ranges of the phase parameter changing $\delta(r)$ practically coincide [Figs. 9(a) and 10(a)]. The histograms $W(\delta)$ are formed by the series of the discrete extrema in the range of the phase shift changing from 0.05π to 2π [Figs. 9(b) and 10(b)]. More equiprobable distribution of the values of the statistical dependencies of local extrema $W(\delta)$ is typical for the kidney tissue sample with the early stage of collagenous disease.

Considerably more obvious differences in the polarization characteristics of the biological tissue images of both types have been discovered within the comparative statistical analysis of the coordinate distributions of their singular points of polarization (Fig. 11). Such analysis included:

- the determination of the linear density of the singular points of polarization in the biological tissue images (the quantity N corresponding to each column of $m_{i=1,2,\ldots,800}$ pixels of CCD camera reception area) (Fig. 12),

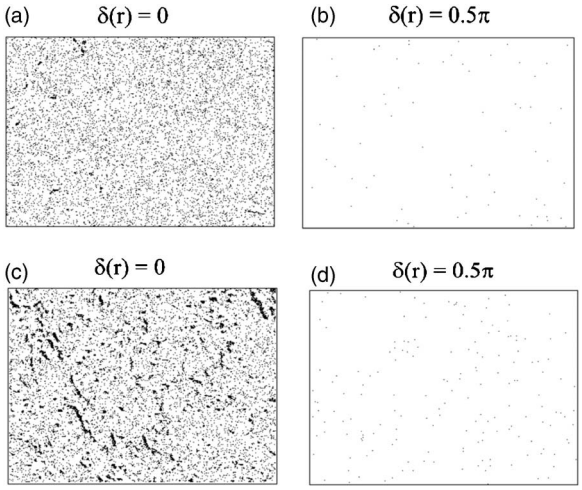

Fig. 11 The coordinate distributions of singly (a), (c) and doubly (b), (d) degenerated polarization singularities of the physically normal (a), (b) and pathologically changed (c), (d) kidney tissue images.

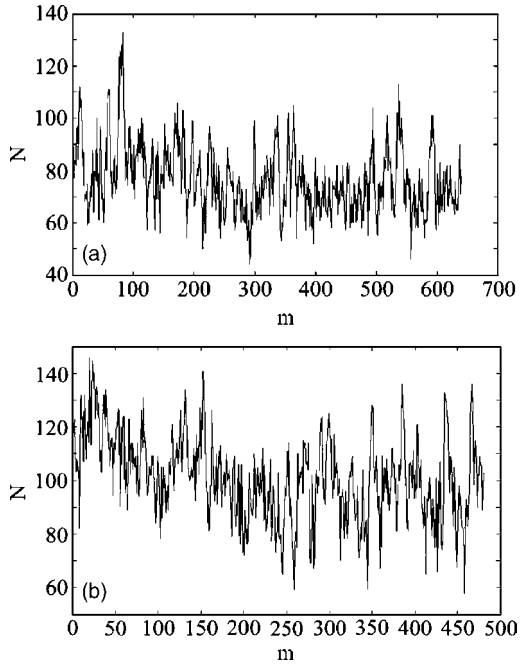

Fig. 12 The linear density of quantity N of singularly polarized points $[\delta(r)=0, \delta(r)=0.5\pi]$ of the physiologically normal (a) and pathologically changed (b) kidney tissue images.

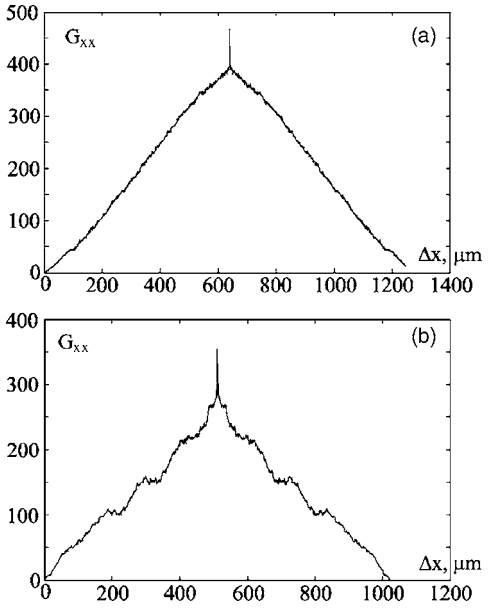

Fig. 13 The autocorrelation functions G_{xx} of the polarization singularities of the physiologically normal (a) and pathologically changed (b) kidney tissue images.

• the calculation of the statistical moments of the first to fourth orders of $N(m)$ dependencies (Table 1),

• the calculation of the autocorrelation functions G_{xx} of dependencies $N(m)$ (Fig. 13),

• the determination of the log-log dependencies ($\log J_{xx}$ versus $\log r^{-1}$) of J_{xx} power spectrums of the autocorrelation functions G_{xx} (Figs. 14 and 15),

• the determination of the inclination angles α_j of the linear sections of $\log J_{xx}$ versus $\log r^{-1}$ dependencies that were obtained by the least-squares technique,[21]

• the self-similarity verification and calculation of the fractal dimensions of $N(m)$ dependencies in accordance with the relation $D(N)=3-\tan \alpha_i$.[23]

The specificity of the linear density changing of singularly polarized points quantity $N(m)$ of the physiologically normal and pathologically changed kidney tissue images has been shown in Figs. 12(a) and 12(b), correspondingly. It is seen from the obtained data that $N(m)$ dependencies for both types of biological tissue images have in general a nonregular, occasional character. It is also obvious that a larger quantity (10 to 15%) of singularly polarized points [Fig. 12(b)] has been involved for the kidney tissue image with an early stage of collagenous disease in comparison with the physically normal biological tissue image [Fig. 12(a)]. More detailed information concerning $N(m)$ distributions character is enclosed in the statistical moments of the first M_N, the second σ_N, the third A_N, and the forth E_N orders (Table 1), which have been calculated in every point $[(X_{m=1+800}, Y_{n=1+600})]$ of the image in accordance with the following relations:

$$M_N = \frac{1}{Q}\sum_{i=1}^{N} N,$$

$$\sigma_N = \sqrt{\frac{1}{Q}\sum_{i=1}^{N} N^2},$$

$$A_N = \frac{1}{\sigma_N^3}\frac{1}{Q}\sum_{i=1}^{N} N^3,$$

$$E_N = \frac{1}{\sigma_N^2}\frac{1}{Q}\sum_{i=1}^{N} N^4, \tag{19}$$

where $Q=mn$ is a total number of pixels of the CCD camera.

The obtained data show that the statistical distribution of singularly polarized points of a healthy kidney biological tissue image is close enough toward the normal one, the asymmetry values A_N and a kurtosis E_N of $N(m)$ distributions are sufficiently low. There is the other picture of $N(m)$ value statistics present in the image of the pathologically changed kidney tissue. The values of the statistical moments of A_N and E_N

Table 1 The statistics of the first to fourth orders of the polarization singularities linear density of the kidney tissue images.

Tissue pattern statistics	Norm (37 patterns)	Pathology (36 patterns)
M_N	0.634±5%	0.706±7%
σ_N	0.198±4%	0.149±6%
A_N	2.689±12%	21.75±15%
E_N	3.8±14%	46.8±18%

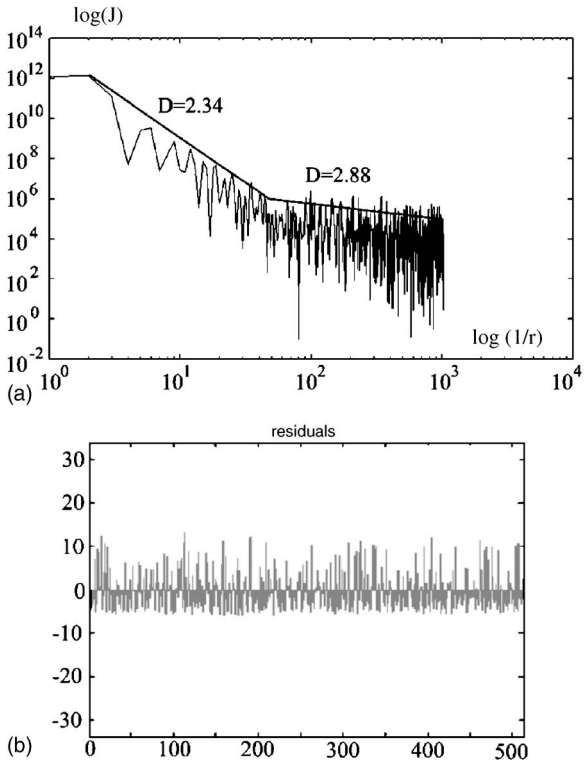

Fig. 14 Log-log dependency of the power spectrum *J* (a) of the linear density of polarization singularities of the physiologically normal kidney tissue. The residuals are shown in fragment (b).

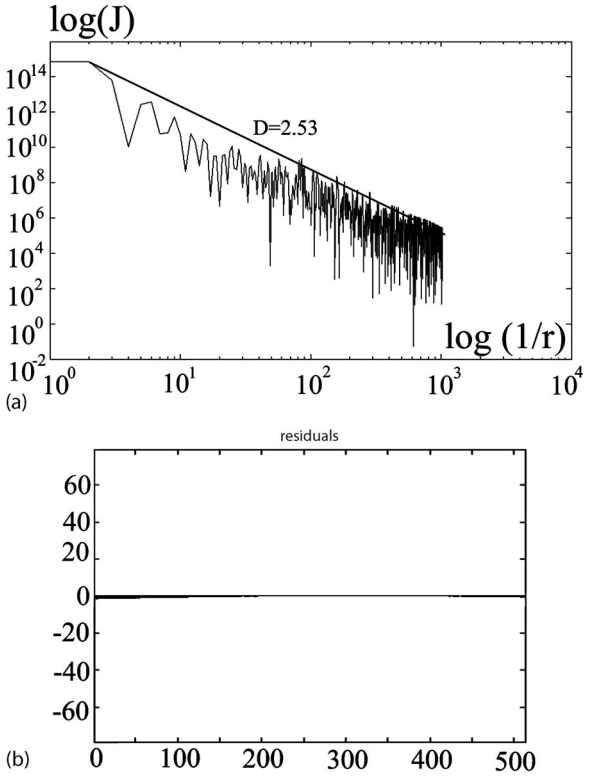

Fig. 15 Log-log dependency of the power spectrum *J* (a) of the linear density polarization singularities of the kidney tissue image with an early collagenous disease. The residuals are shown in fragment (b).

are practically increasing on one level that indicates the abrupt change in the statistics of the line density dependency of singular points quantity. The similar information is enclosed in the comparative analysis of the autocorrelation functions G_{xx} of both types of sample images (Fig. 13).

For depicting the physiologically normal kidney tissue, the dependency G_{xx} has monotonously lowering tendency [Fig. 13(a)] that proves the presence of an occasional coordinate structure of the polarization singularities. The correlation structure of the singular polarization points of the kidney tissue image with an early stage of collagenous disease is a different one. The autocorrelation function G_{xx} has been modulated by a harmonic component [Fig. 13(b)] that points to the presence of an additional regular (ordering) component in the coordinate distribution of polarization singularities.[19]

The discovered changes in the statistics of the polarization singularities might be connected with the modification of the kidney tissue morphological structure when the physiological condition of the kidney tissue was being changed. The morphology of the kidney tissue could be represented by a double-component amorphous-crystalline structure. A crystalline amorphous structure consists of two layers: an exterior cork tissue and an internal medulla. The crystalline one is represented by the epithelium tubules with its optical anisotropic substance and consists of numerous chaotically located capillary nodes. The formation of an additional connecting tissue (collagenous disease) is characterized by the definite directions of growth and the enlargement of the epithelium layers. From the optical point of view, such processes are escorted by the phase-shift value increasing $\delta(r)$ and, consequently, a corresponding number of the singularly polarized points in the image of the pathologically changed kidney tissue [Figs. 12(a) and 12(b)]. On the other hand, in the coordinate structure of such points, the "regular" component has been formed. That is why the asymmetry A_N and the kurtosis E_N of the distributions $\delta(r)=0$, $\delta(r)=0.5\pi$ increase abruptly, and in the autocorrelation dependencies G_{xx}, a harmonic component appears [Fig. 13(b)].

The obtained information concerning the differences in the statistics of coordinate distributions $\delta(r)=0$, $\delta(r)=0.5\pi$ of both types of the kidney tissue images has been added by the analysis of their self-similarity degree.

Figures 14(a) and 15(a) represent the dependencies, $\log(J_{xx})$ versus $\log(r^{-1})$, received for the coordinate distributions of the polarization singularities of the physiologically normal and as well as the pathologically changed kidney tissue images.

The analysis of the obtained data showed that the approximation of the dependencies of $\log(J_{xx})$ versus $\log(r^{-1})$ by the least-squares technique [Figs. 14(b) and 15(b)] for the polarization singularities distribution of images of the physiologically normal kidney biological tissue gives a set of the broken lines with a number of the local inclinations α_j [Fig. 14(a)]. The polarizationally singular structure of the pathologically changed tissue is a self-similar (fractal): the statistical processing of the dependencies $\log(J_{xx})$ versus $\log(r^{-1})$ gives the direct line with one stable inclination α [Fig. 15(a)].

Conclusions

1. The analytical conditions of the formation of singly and doubly degenerated polarization singularities and experimentally investigated statistical characteristics of their coordinate distributions in the biological tissue images of a different morphological structure and physiological condition have been determined.

2. It has been shown that the third and the fourth statistical moments of the linear density of the singular points of polarization are the most sensitive toward the optical-geometric structure of the biological tissue.

3. It was determined that the coordinate structure of the polarization singularities of the physiologically normal biological tissue image is random while the coordinate structure of the pathologically changed biological tissue is a self-similar (fractal) one.

References

1. G. G. Stokes, "On the composition and resolution of streams of polarized light from different sources," *Trans. Cambridge Philos. Soc.* **9**, 399 (1852); G. G. Stokes, *Mathematical and Physical Papers*, Vol. 3, p. 233, Cambridge University Press, Cambridge (1922).
2. M. Born and E. W. Wolf, *Principles of Optics*, Pergamon Press, Oxford (1959).
3. J. F. Nye, *Natural Focusing and the Fine Structure of Light*, Institute of Physics Publishing, Bristol (1999).
4. J. F. Nye, "Polarization effects in the diffraction of electromagnetic waves: The role of disclinations," *Proc. R. Soc. London, Ser. A* **387**, 105–132 (1983).
5. I. Freund, "Bichromatic optical Lissajous fields," *Opt. Commun.* **226**, 351–376 (2003).
6. J. F. Nye and J. V. Hajnal, "The wave structure of monochromatic electromagnetic radiation," *Proc. R. Soc. London, Ser. A* **409**, 21–36 (1987).
7. M. V. Berry and M. R. Dennis, "Polarization singularities in isotropic random vector waves," *Proc. R. Soc. London, Ser. A* **457**, 141–155 (2001).
8. A. D. Dolgov, A. G. Doroshkevich, D. I. Novikov, and I. D. Novikov, "Classification of singular points in the polarization of the cosmic microwave background and eigenvectors of the Stokes matrix," *JETP Lett.* **69**, 427–433 (1999).
9. A. I. Konukhov and L. A. Melnikov, "Optical vortices in a vector fields: The general definition based on the analogy with topological solitons in a 2D ferromagnet, and examples from the polarization transverse patterns in a laser," *J. Opt. B: Quantum Semiclassical Opt.* **3**, S139–S144 (2001).
10. I. Freund, "Poincare vortices," *Opt. Lett.* **26**, 1996–1998 (2001).
11. J. F. Nye, "Lines of circular polarization in electromagnetic wave fields," *Proc. R. Soc. London, Ser. A* **389**, 279–290 (1983).
12. I. Freund, "Coherency matrix description of optical polarization singularities," *J. Opt. A, Pure Appl. Opt.* **6**, S229–S234 (2004).
13. S. C. Cowin, "How is a tissue built?," *J. Biomed. Eng.* **122**, 553–568 (2000).
14. O. V. Angelsky, Yu. Ya. Tomka, A. G. Ushenko, Ye. G. Ushenko, and Yu. A. Ushenko, "Investigation of 2D Mueller matrix structure of biological tissues for pre-clinical diagnostics of their pathological states," *J. Phys. D* **38**, 4227–4235 (2005).
15. A. G. Ushenko and V. P. Pishak, "Laser polarimetry of biological tissue. Principles and applications," in *Coherent-Domain Optical Methods: Biomedical Diagnostics, Environmental and Material Science*, V. Tuchin, Ed., pp. 67–93, Kluwer Academic Publishers, Norwell, MA (2004).
16. O. V. Angelsky, A. G. Ushenko, S. B. Ermolenko, D. N. Burcovets, V. P. Pishak, and Yu. A. Ushenko, "Polarization-based visualization of multifractal structures for the diagnostics of pathological changes in biological tissues," *Opt. Spectrosc.* **89**, 799–804 (2000).
17. E. I. Olar, A. G. Ushenko, and Yu. A. Ushenko, "Correlation microstructure of the Jones matrices for multifractal networks of biotissues," *Laser Phys.* **14**, 1012–1018 (2004).
18. E. I. Olar, A. G. Ushenko, and Yu. A. Ushenko, "Polarization correlation measurements of the phase tomograms of optically anisotropic biofractals," *Laser Phys.* **14**, 1115–1121 (2004).
19. O. V. Angelsky, G. V. Demyanovsky, A. G. Ushenko, D. N. Burcovets, and Yu. A. Ushenko, "Wavelet analysis of two-dimensional birefringence images of architectonics in biotissues for diagnosing pathological changes," *J. Biomed. Opt.* **9**, 679–690 (2004).
20. O. V. Angelsky, A. G. Ushenko, D. N. Burcovets, and Yu. A. Ushenko, "Polarization visualization and selection of biotissue image two-layer scattering medium," *J. Biomed. Opt.* **10**, 014010 (2005).
21. O. V. Angelsky, A. G. Ushenko, and Yu. A. Ushenko, "Polarization reconstruction of orientation structure of biological tissues birefringent architectonic nets by using their Mueller-matrix speckle-images," *J. Holography Speckle* **2**, 72–79 (2005).
22. O. V. Angelsky, A. G. Ushenko, Yu. A. Ushenko, Ye. G. Ushenko, Yu. Ya. Tomka, and V. P. Pishak, "Polarization-correlation mapping of biological tissue coherent images," *J. Biomed. Opt.* **10**, 064025 (2005).
23. D. J. Whitehouse, "Fractal or fiction?," *Wear* **249**, 345–353 (2001).